Petroleum 11 (2025) 158–173

Contents lists available at ScienceDirect

Petroleum

journal homepage: www.keaipublishing.com/en/journals/petlm

Full Length Article

# Exploring hydrocarbon potential with 3D modeling techniques: Lower Cretaceous formations in Abu Sennan field, north Western Desert

Taher Mostafa [a], Mohamed Reda [a, *], Mohamed Mosaad [a], Dmitriy Martyushev [b, **], Mansour H. Al-Hashim [c], Mohamed Fathy [a]

[a] Al-Azhar University, Faculty of Science, Geology Department, P.O. Box 11884, Cairo, Egypt
[b] Department of Oil and Gas Technologies, Perm National Research Polytechnic University, Perm, 614990, Russia
[c] Department of Geology and Geophysics, College of Science, King Saud University, 2455, Riyadh 11451, Saudi Arabia

ARTICLE INFO

*Article history:*
Received 2 August 2024
Received in revised form
25 January 2025
Accepted 10 March 2025

*Keywords:*
Seismic interpretation
Petrophysical analysis
Reservoir modeling
Abu Sennan field
Western Desert

ABSTRACT

The northern portion of the Egyptian Western Desert is a very promising oil-producing province. The Abu Roash and Bahariya formations in Abu Sennan Field have a diverse lithological composition, leading to variances in reservoir continuity both horizontally and vertically. The reservoir heterogeneity problem is addressed by utilizing datasets derived from five wells and 3D seismic data that covers the full region of Abu Sennan. The lithology and reservoir levels were determined using geophysical well data. The investigated formations consist of sandstone, carbonate, and shale. The "E" and "G" members of the Abu Roash Formation, in addition to the Bahariya Formation, have the highest potential for containing hydrocarbons. Abu Roash E has a range of net pay from 17–47 m, shale volume ranging from 17% to 36%, effective porosity ranging between 20% and 26%, and oil saturation ranging between 49% and 77%. The Abu Roash "G" has a net pay range of 7–34 m, a shale content ranging from 5% to 42%, an effective porosity between 10% and 24%, and a hydrocarbon saturation ranging from 46% to 60%. The Bahariya Formation has a vertical thickness of 12–62 m, with a percentage of shale ranging from 16% to 44%. The formation also exhibits an effective porosity ranging from 15% to 26% and an oil saturation ranging between 46% and 77%. Analyzed 3D seismic data were utilized to create depth-structure maps. Seismic data interpretation and petrophysical analysis enabled the creation of 3D models for the structures and reservoirs in the Abu Sennan region. The static models served as the main inputs for calculating the volumetrics and generating two additional interesting opportunities in the researched region. For the investigated reservoirs, the estimated stock tank oil in place was about 394, 216, 376, and 601 ($\times 10^6$ $m^3$) for AR/E, AR/F, AR/G, and Upper Baharyia, respectively. The projected volumes show the potential of the investigated intervals.



## 1. Introduction

The discovery and production of hydrocarbons, including oil and natural gas, have been crucial in fostering economic expansion, industrial development, and technical progress. The Egyptian Western Desert is the site of recent hydrocarbon discoveries as reported by many scholars [1–5]. After a lengthy history of investigation, potential reservoir and source rocks, such as the Upper Cretaceous Bahariya and Middle Jurassic Khatatba formations, have been discovered in Egypt's Western Desert [4,6–11]. The significant thickness of the sedimentary layers, particularly the primary reservoirs in the Western Desert, along with the valuable results of source rock analysis, have led to the recognition of the Abu Gharadig Basin as the primary producing basin in the northern area of the Western Desert [12–18]. The Abu Sennan oil field is situated in the eastern section of the Qattara Depression, which is part of the Abu Gharadig Basin. It is located between latitudes 29°30′N and 29°40′N and longitudes 28°30′E and 28°40′E (Fig. 1), covering approximately 300 $km^2$ and being approximately 200 km west of the Nile River and 20 km south of the Abu Gharadig Gas Field [19–25].

The Abu Roash and Bahariya formations contain several rock types, and the characteristics of the reservoirs vary in both horizontal and vertical directions [26,27]. Many authors have studied the Abu

* Corresponding author.
** Corresponding author.
*E-mail addresses:* mohamedreda.88@azhar.edu.eg (M. Reda), martyushevd@inbox.ru (D. Martyushev).

Peer review under the responsibility of Southwest Petroleum University.

https://doi.org/10.1016/j.petlm.2025.03.004

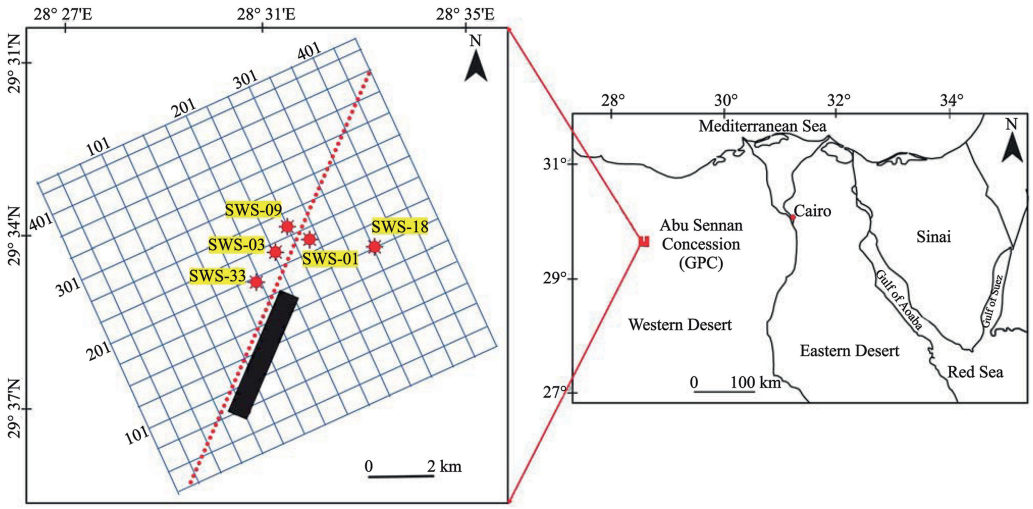


**Fig. 1.** The map showing the location of the Abu Sennan oilfield as well as the seismic lines and wells.

Gharadig Basin from different viewpoints [12,19–25,28–31]. An extensive analysis of the components and mechanisms of the petroleum system has revealed the most potential for petroleum in the Abu Sennan region, with the Bahariya Formation serving as the reservoir [32]. This study uses well logs and seismic data to identify and evaluate reservoir intervals, constructing 3D static models using a variety of modeling methodologies via Petrel software [33–36]. While the previously mentioned study investigated only the Bahariya Formation as a reservoir rock, the current study focuses on both Abu Roash and Bahariya reservoirs. This research uniquely focuses on assessing the potential of the Abu Roash and Bahariya reservoirs in the Abu Sennan Field. The primary goal is to integrate geological, geophysical, and petrophysical data to construct three-dimensional static reservoir models, enabling a thorough evaluation of hydrocarbon capacity. Additionally, the study aims to estimate oil recovery potential and total reserves, while identifying new opportunities for field development [37–40]. These findings will support strategies to boost production rates and provide critical insights for formulating a development plan for the Abu Sennan oil field.

## 2. Geologic settings

Tethyan rifting transformed the Abu Gharadig Basin into a large, half-graben basin during the Jurassic period. It then sank throughout the Cretaceous period. Subsequently, the half-graben underwent inversion as a result of the Syrian Arc Deformation, which caused significant destruction in northern Egypt during the Late Cretaceous period. This research specifically examines the Bahariya and Abu Roash formations, which serve as the main reservoirs for oil production in the Abu Sennan region.

These formations have been the subject of several previous studies [30–32,41–43]. A study by Ref. [44] concluded that the northern part of Egypt was subjected to three tectonic events. The first event, which occurred during the Paleozoic–Triassic period, resulted in a northwest or west-northwest structural trend. The second event, which took place during the Cretaceous period, was caused by the east-northeast Syrian Arc system. The third event, occurring during the Late Eocene–Early Oligocene period, led to the formation of a northwest structural direction in the Gulf of Suez and a north-northeast Aqaba direction (Fig. 2).

Said, 2017 indicated that normal fault-controlled structures influence the northern region of the Western Desert. The analysis of seismic and well-log data can help identify and understand these structures. In the northern portion of the Western Desert, the underlying geological formation is made up of a series of structurally elevated areas that run NNW–SSE and a series of structurally depressed areas that run in the same direction (along the Gulf of Suez). Extensive zones of structures trending NE–SW (Syrian Arc System) complicate this structure. The NW–SE trend is reported in several Tertiary surface structures lying NE of Siwa and extending along Moghra, Wadi El-Natrun, and the Nile Delta [46]. During the Early Jurassic and Cretaceous eras, the Abu Sennan region saw a sequence of normal faults that were aligned in a northeast to southwest direction [47,48]. Abu Sennan anticlines were formed during the Late Cretaceous–Middle Eocene epoch as a result of structural inversion occurring in these faults.

The lithostratigraphic sequence of the Abu Gharadig Basin spans from the Precambrian to the Quaternary period [49], and the lithostratigraphic section in Abu Sennan field is similar to the northern Western Desert (Fig. 3). The stratigraphic column in the Abu Sennan oil field shows that the Khatatba Formation, which consists of sandstone, shale, and limestone, is found in the Middle Jurassic. It is situated above the Wadi El-Natrun Formation, which is primarily composed of sandstone and shale, in the Lower Jurassic. The Khatatba Formation also underlies the Masajid Formation, which is made up of limestone and shale, in the Lower Cretaceous [4,50,51] Limestone and sandstone make up the Alam El-Beuieb Formation, which is located unconformably above the Masajid Formation and unconformably under the Alamine Dolomite Formation, both of which are part of the Lower Cretaceous [50,51]. The Alamine Dolomite Formation conformably underlies the Dahab Shale and Kharita Formations comprising sandstone and shale. The Bahariya Formation of the Upper Cretaceous is primarily composed of sandstone, with thin layers of shales and limestone [41,42]. The formation unconformably rests above the Kharita Formation and conformably sits below the Upper Cretaceous Abu Roash Formation. The Bahariya Formation is split into seven members (A, B, C, D, E, F, and G) and is composed of limestone with sandstone and shale intercalations. The Abu Roash Formation is found beneath the Upper Cretaceous Khoman Formation, with an unconformity between them. The Khoman Formation consists of chalk and shale. The Dabaa Formation, which is of Middle Eocene-Oligocene age, is composed of shale and is found on top of the Paleocene-Eocene Appolonia Formation, which comprises of limestone and shale, in a conformable manner [52–54]. It underlies the Miocene Moghra Formation, which is composed of sandstone, shale, and limestone. As stated by Ref. [45], the east-west elongated intra-cratonic rift basin links to the Abu Gharadig Basin.

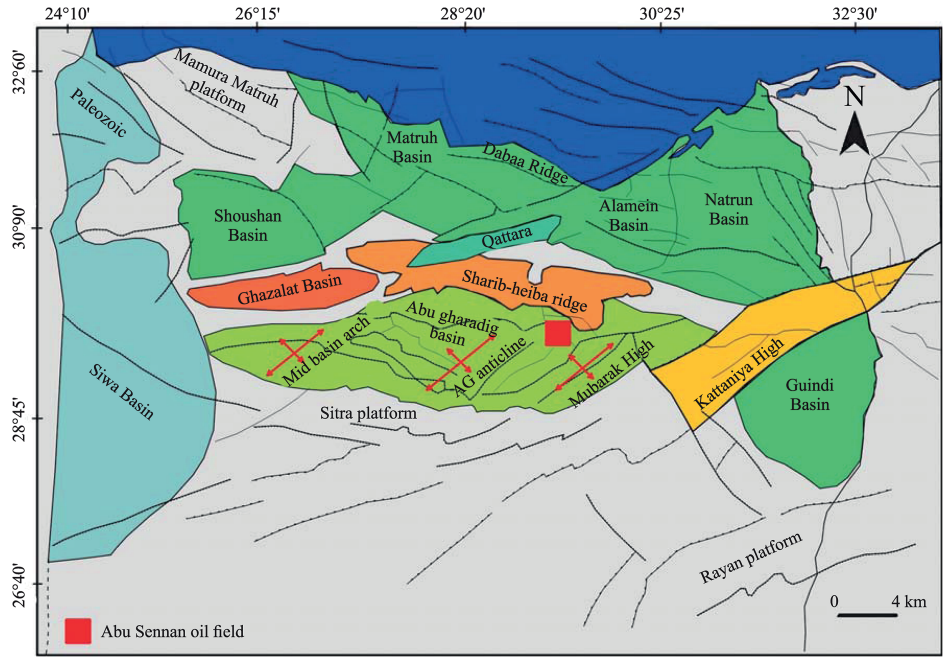


**Fig. 2.** The location map shows the different basins of the northern part of the Western Desert. The small red square represents the studied General Petroleum Company concession, Abu Gharadig Basin, north of the Western Desert modified after [45].

## 3. Materials and methods

A complete set of records for five wells, penetrating reservoir layers in the investigated area, and a 3D seismic volume covering the entire Abu Sennan field (Fig. 1), were used to conduct this integrated study (evaluating reservoir layers, modeling the structural framework, and building 3D static facies and property models of the reservoirs). A detailed description of the used data and applied methods is provided through the following points.

### 3.1. Well logging data

For the current investigation, four wells in the examined region were provided with a comprehensive set of logs, including gamma-ray (GR), resistivity, neutron, density, and acoustic logs, in both Las and Asci formats. The well logs given enabled the qualitative and quantitative identification, examination, and evaluation of the petrophysical parameters of the hydrocarbon-bearing formations (Abu Roash and Bahariya formations) in the area under study.

### 3.2. Lithological identification

The lithological compositions of the formations under study were determined by analyzing the data from several geophysical logs, including gamma ray, resistivity, density, and neutron logs. Additionally, lithological identification graphs such as *M*–*N* and Neutron-density cross plots were utilized [56,57]. The *M*–*N* cross plot utilizes density, compensated neutron, and acoustic data to identify binary and ternary mineral combinations [17,18,34,51,58–60]. This technique employs the properties of fluid and log characteristics, which are combined in the three porosity logs: sonic, density, and neutron. The *M*–*N* cross plot, sometimes referred to as the Tri-porosity plot, is a visual tool employed for the analysis of the relation between *M* and *N* parameters. The cross plot technique is employed to identify the mineral composition inside intricate lithological formations. The porosity logs are utilized to compute two functions (*M* and *N*) that are not influenced by the main porosity. Consequently, plotting these two numbers against each other allows for a broad lithologic categorization [35,61]. The *M*–*N* plot may be used to identify minerals and assess the lithologic composition of each zone in relation to the standard *M*–*N* values of common minerals and rocks [61–63]. The definitions of *M* and *N* are as follows:

$$N=(\Phi_{Nfl}-\Phi_{Nlog})/(\rho_b-\rho_{fl}) \quad (1)$$

$$M=(\Delta t_{fl}-\Delta t_{log})/(\rho_b-\rho_{fl})\times 0.01 \quad (2)$$

where:
$\Phi_{Nfl}$ is neutron porosity of the fluid (typically that of water, used as a reference),
$\Phi_{Nlog}$ is neutron porosity value read from the log,
$\rho_b$ is bulk density, g/cm$^3$,
$\rho_{fl}$ is fluid density, g/cm$^3$,
$\Delta t_{fl}$ is sonic travel time (transit time) of the fluid, μs/ft,
$\Delta t_{log}$ is sonic travel time measured from the log, in μs/ft.

The other graph used for lithological identification in this study is the Neutron-density cross plot.

### 3.3. Shale volume calculation

The volume of shale was determined in the present study by applying Eq. (3) and analyzing the gamma-ray log.

$$V_{shGR}=(GR_{log}-GR_{min})/(GR_{max}-GR_{min}) \quad (3)$$

where:
$V_{shGR}$ is volume of shale calculated from the gamma-ray log,
$GR_{log}$ is gamma-ray value from the well log at a particular depth,
$GR_{min}$ is minimum gamma-ray value (typically clean sand baseline),
$GR_{max}$ is maximum gamma-ray value (shale baseline).

### 3.4. Porosity and fluid saturation calculation

The presence of neutron and density logs in the available well-logged data allowed for the computation of both total and effective

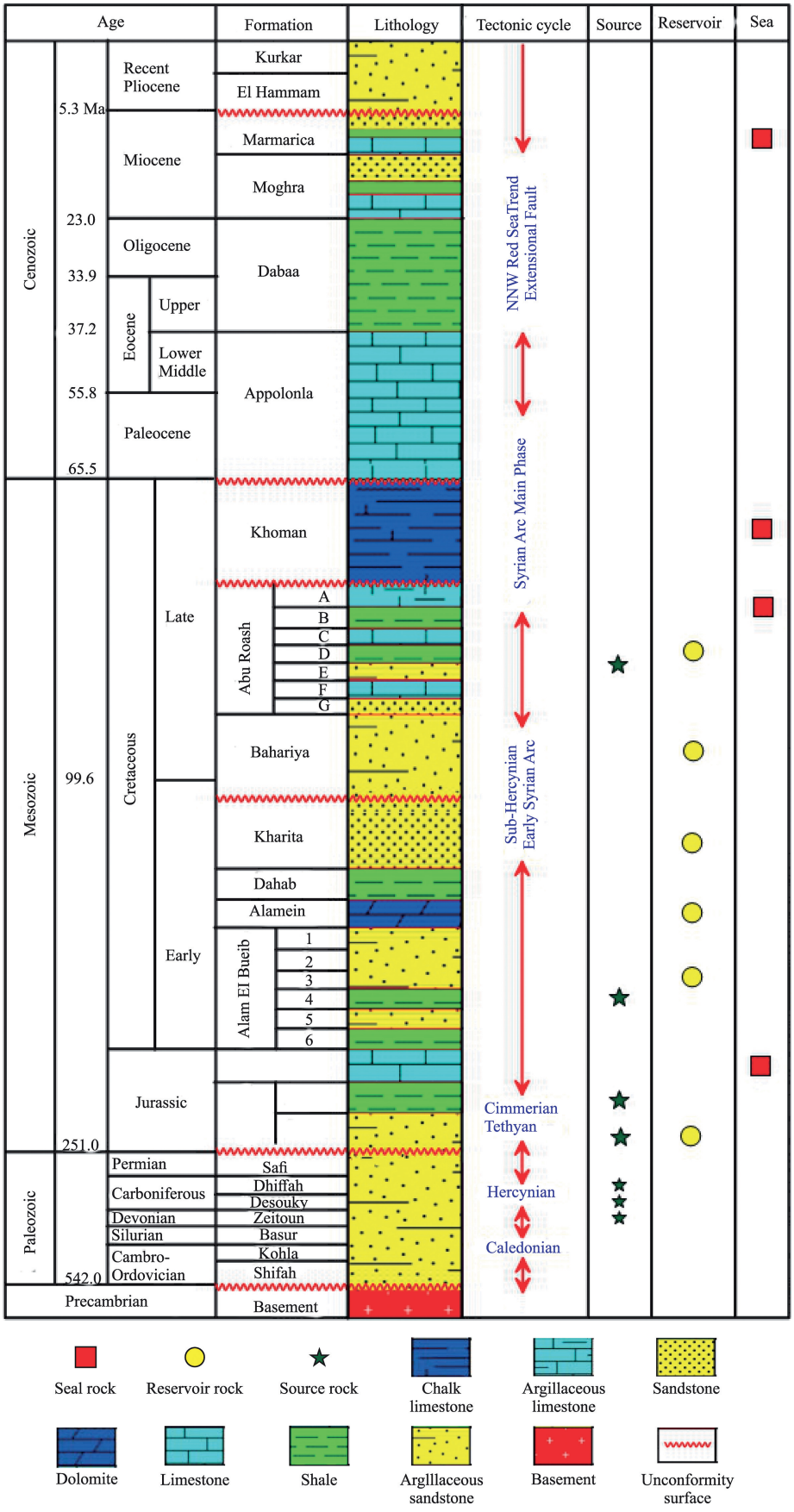


**Fig. 3.** A generalized lithostratigraphic column of the Abu Sennan oil field, in the Abu Gharadig Basin illustrating the possible petroleum system elements in the study area modified after [52,55].

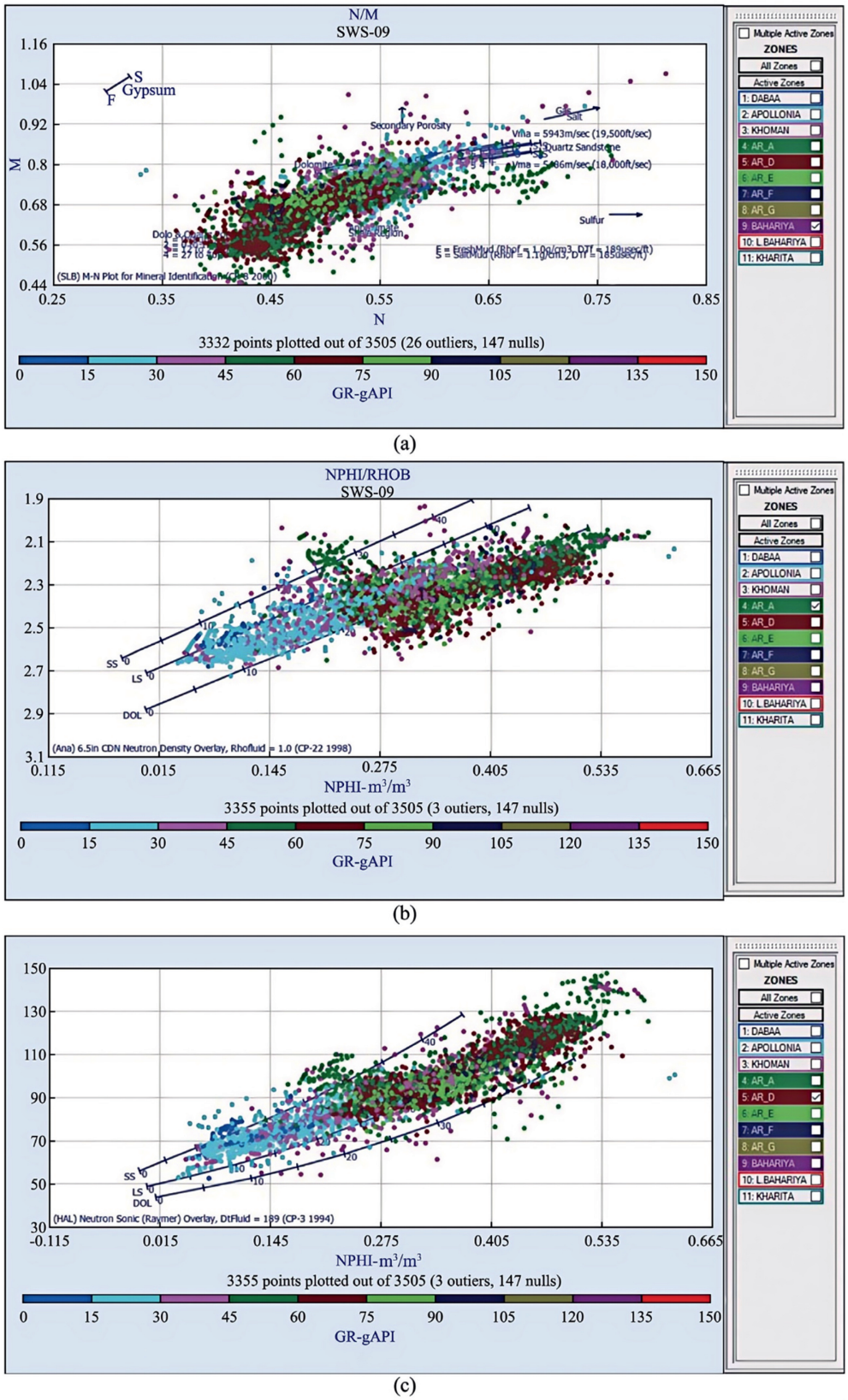


**Fig. 4.** Lithological identification cross plots of the studied reservoirs: (a) mN cross plot, (b) neutron-density, and (c) neutron-sonic.

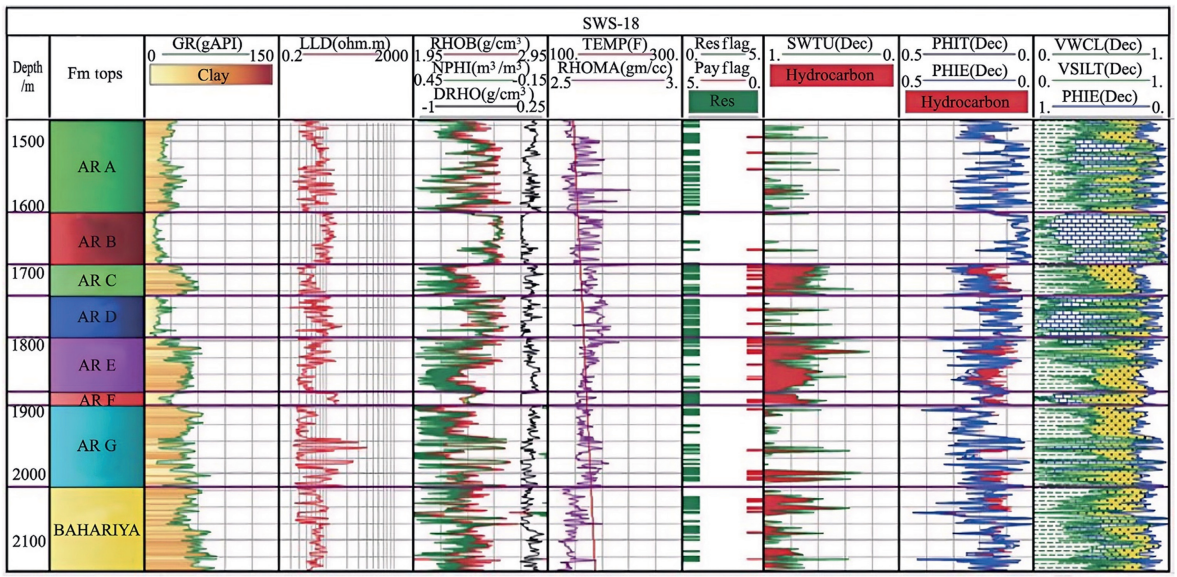


**Fig. 5.** Lithosaturation panel representing the computer processed interpretation (CPI) and manifesting the vertical distribution of the calculated petrophysical parameters (shale volume, effective porosity, and saturation).

porosity using the neutron-density model. The previously determined shale volume allowed for the determination of the effective porosity, a portion of the overall porosity. The resistivity of the formation water, $R_w$, was calculated through Pickett's plot, which included plotting porosity against deep resistivity [64]. Given that the reservoirs under investigation consist of sandstones with a high clay content, the dual-water model was employed to estimate the saturation of water. This explanation describes how clay minerals impact the resistivity of the reservoir rock, according to the dual-water hypothesis, which states that the reservoir contains two kinds of fluids: bound water inside the clay matrix and free water in the rock's pore spaces [65]. Developing a reliable explanation for the conduction that takes place within the surface volume of the clay mineral was the primary motivation for developing the dual-water model. We aimed to take conductivity into account in the double layer, its immediate vicinity, and the unaffected clay layer. The dual-water model is an improvement on the Waxman-Smits model that accounts for saturation of water. Assuming the identical conduction geometry of free water and clay counterions, it functions [66]. The dual-water model equation is as follows:

$$\frac{1}{R_t} = \frac{S_w^n}{F_0}\left[\frac{1}{R_w} + \frac{V_Q Q_V}{S_{wt}}\left(\frac{1}{R_{cw}} - \frac{1}{R_w}\right)\right] \quad (4)$$

**Table 1**
The resulted petrophysical parameters calculated for Abu Roash members and Baharyia Formation.

| Well | Fm. or member | Net pay [m.] | Clay volume [%] | Effective porosity [%] | Oil saturation [%] |
|---|---|---|---|---|---|
| SWS-01 | AR/C | 9.25 | 58 | 20 | 79 |
| | AR/D | 19.75 | 30 | 27 | 81 |
| | AR/E | 24 | 36 | 25 | 77 |
| | AR/F | 14.5 | 19 | 19 | 81 |
| | AR/G | 7 | 42 | 10 | 75 |
| | Baharyia | 27.5 | 44 | 15 | 77 |
| SWS-03 | AR/C | 4.12 | 27 | 20 | 45 |
| | AR/D | 10 | 8 | 21 | 62 |
| | AR/E | 47.5 | 24 | 25 | 49 |
| | AR/F | 15 | 2 | 22 | 68 |
| | AR/G | 15 | 12 | 23 | 46 |
| | Baharyia | 28 | 24 | 22 | 46 |
| SWS-09 | AR/C | – | – | – | – |
| | AR/D | 5.13 | 3 | 16 | 68 |
| | AR/E | 38.15 | 21 | 20 | 56 |
| | AR/F | 3.79 | 6 | 20 | 66 |
| | AR/G | 33.86 | 15 | 21 | 55 |
| | Baharyia | 62.35 | 24 | 18 | 48 |
| SWS-18 | AR/C | 16.5 | 19 | 24 | 48 |
| | AR/D | 2.1 | 2 | 24 | 46 |
| | AR/E | 17.4 | 18 | 26 | 54 |
| | AR/F | 4.5 | 17 | 19 | 43 |
| | AR/G | 12.5 | 5 | 24 | 56 |
| | Baharyia | 12.5 | 21 | 26 | 46 |
| SWS-33 | AR/C | 8.9 | 14 | 26 | 51 |
| | AR/D | 11.2 | 8 | 24 | 52 |
| | AR/E | 31.42 | 22 | 22 | 54 |
| | AR/F | 5.47 | 5 | 22 | 43 |
| | AR/G | 18.44 | 12 | 24 | 60 |
| | Baharyia | 14.33 | 16 | 17 | 47 |

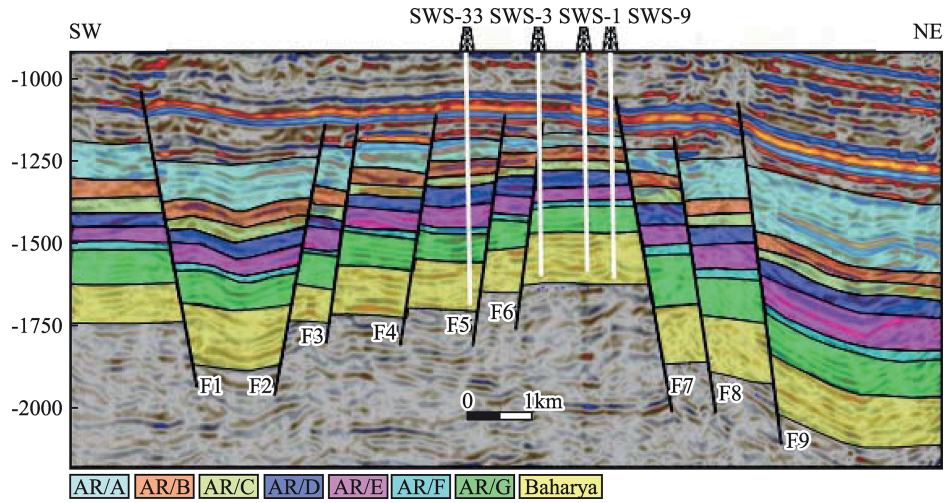


**Fig. 6.** An interpreted NE–SW-trending seismic section illustrating the different trends of the normal faults affecting Abu Sennan.

The variable $R_t$ indicates the deposit's resistivity. $R_w$ refers to the water resistivity, whereas $R_{cw}$ refers to the clay-bound-water resistivity. $Q_v$ represents the effective concentration of clay counterions, while *VQ* represents the volume of the clay-water mixture. The formation resistivity factor is denoted as $F_0$. The hydrocarbon saturation was determined by applying the following equation after determining the water saturation:

$$S_{hr} = 1 - S_w \quad (5)$$

After calculating the petrophysical parameters, both vertical and lateral distribution of the output results were conducted via the lithosaturation panel and iso-parametric contour maps, respectively.

### 3.5. Seismic data analysis

A 3D seismic volume was used to characterize the subsurface structural settings and model a 3D structural framework of the area. The first and the most crucial step in the seismic data interpretation process is the seismic-well tie step. The presence of more than one check shot survey permits an accurate seismic-well tie. Using this tie, the tops of the studied surfaces were identified and then picked all over the study area. The interpreted horizons of interest enabled the creation of structure contour maps to generate new prospects. Computer-based seismic analysis was conducted to identify the structural framework, map the chosen formations, and evaluate the hydrocarbon potentiality of the investigated reservoirs, the Abu Roash and Bahariya formations. The first step in seismic data analysis is a seismic-well tie. This step was accomplished using the provided check-shot survey in the study area. After applying the tie and identifying the tops of the targeted formations, a 3D horizon tracing for the targets was accomplished, and the data were used to interpret the affected structure. The faults affecting the area were easily identified, interpreted, and picked. Three primary fault trends were recognized. Time-structure maps were constructed for the studied horizon. After that, a time-depth conversion was conducted utilizing the time-depth relation obtained from the given checkshot data to create depth-structure maps for the same horizons.

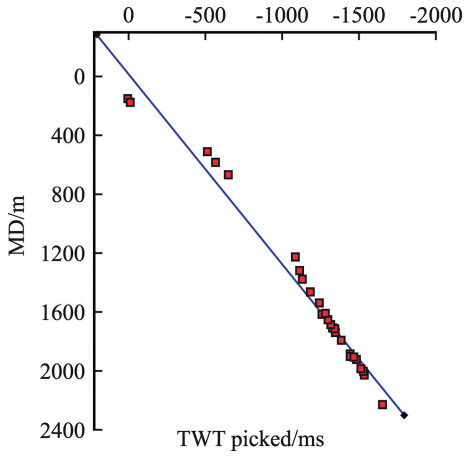


**Fig. 7.** The time-depth relation used for the time-depth conversion.

### 3.6. Reservoir modeling

Since building the structure, facies, and property models is the primary tool to attain this study's objective, integrating seismic and petrophysical data was accomplished, as they represent the backbone of the facies and property modeling [51,67,68]. Integrated petrophysics and seismic data are used to determine the ranges of lithotypes and rock properties through Petrel software. Static reservoir modeling is a powerful tool for outlining reservoir boundaries. 3D static reservoir modeling is used for the studied reservoir, starting with building a facies model using various logs from the wells penetrating the reservoir levels and ending with establishing the petrophysical, porosity, and saturation modeling of the investigated reservoirs in the study area.

### 3.7. Structural modeling

This study considered the fault-modeling, pillar-gridding, horizon-making, and layering processes. Pillar-gridding is primarily used to create a skeletal fault framework to guide the grid framework by aligning cells parallel to the fault and transforming them into surfaces. These cells can be used for geomodeling and static modeling in addition to flow simulation. The interpreted horizons are used for horizon making step and after that, each layer was subdivided into sublayers which is called layering process [51].

### 3.8. Facies and petrophysical modeling

Comprehensive equations were used to create a discrete facies log from the log responses for the studied intervals. This log was upscaled and finally distributed over the area using stochastic

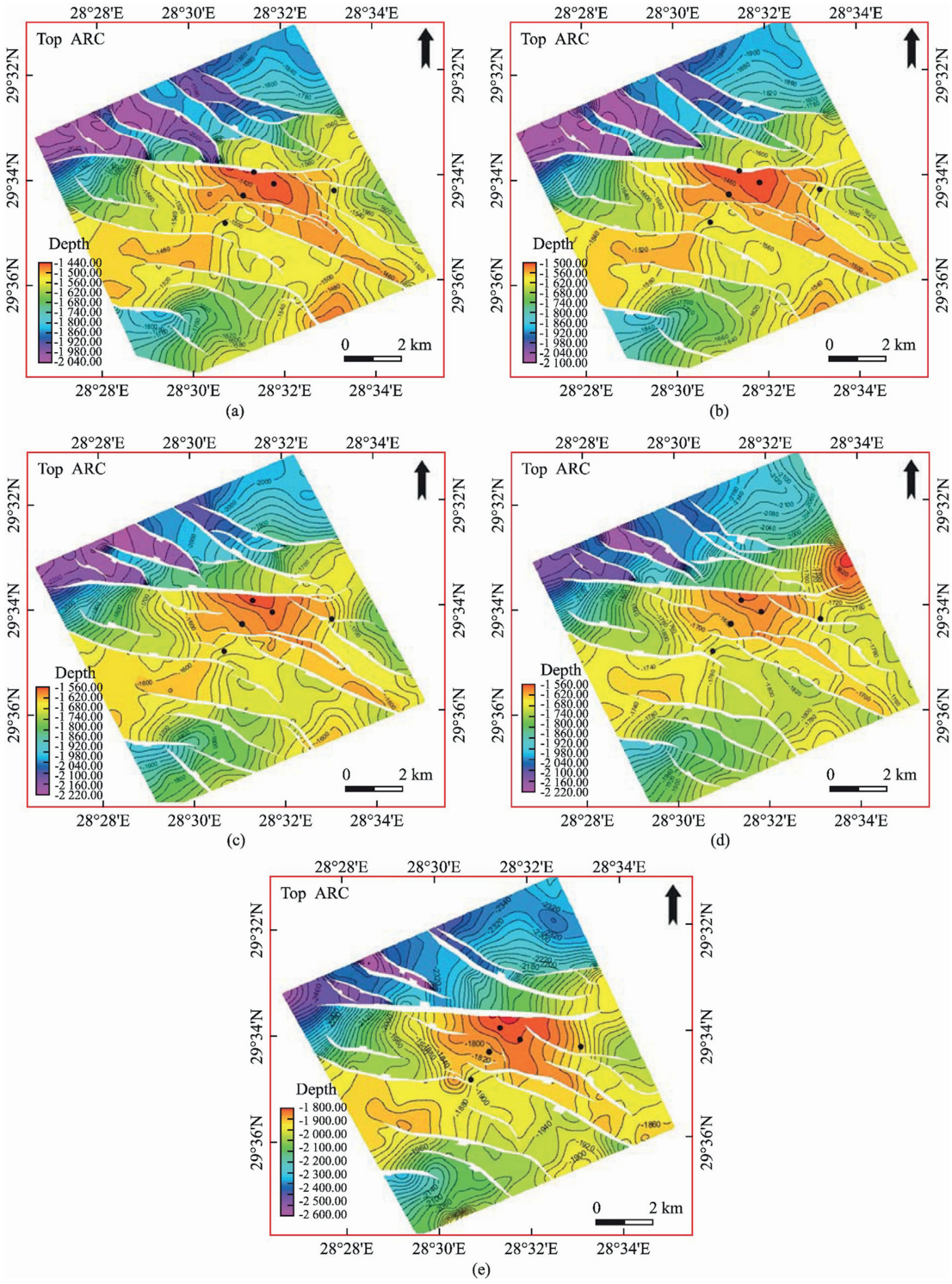


**Fig. 8.** Depth-structure contour maps illustrating the subsurface structure on top: (a) Abu Roash C, (b) Abu Roash D, (c) Abu Roash E, (d) Abu Roash G members, and (e) the Bahariya Formation.

methods. Facies typing and analysis are crucial in choosing satisfactory techniques used in property modeling, [69]. The property modeling is done by using the upscaled log-derived petrophysical parameters and spreading them out in the area based on how the facies are distributed. To properly characterize static reservoirs, whether continuous or discontinuous, it is essential to spread these properties throughout the grid by giving a value to each cell. We used the facies distribution to help us generate fresh drilling possibilities. Analyzing the geophysical data given for the wells in the study zone allowed us to establish the effective porosity and oil saturation. After that, these parameters were spread out across all the wells via extrapolation. First, structural and facies models served as guides for developing the effective porosity and oil saturation models, which in turn used the parameters [53].

### 3.9. Volumetric calculations

3D static reservoir models are vital and function as the primary tool to estimate any reservoir's oil and gas volumes. The following equation was employed to calculate the oil initially in place (OIIP) in stock barrels [70,71].

$$OIIP = (GRV \times Ø \times NTG \times S_{oil})/FVF \quad (6)$$

The variables in question are defined as follows: *GRV* represents the gross rock volume, *Ø* represents the effective porosity, *NTG* represents the net to gross ratio, $S_{oil}$ represents the oil saturation, and *FVF* represents the formation volume factor.

Oil–water contact surfaces are essential for volumetrics; therefore, they were identified and outlined using the interpretation of well-log responses for each promising reservoir in the area.

## 4. Results

### 4.1. Well logs interpretation

The lithological compositions of the examined formations were determined using NM, neutron density, and neutron-sonic cross-plots as shown in Fig. 4(a)–(c) respectively. A computer-processed analysis was performed on potential reservoir levels in the area being studied through the interactive petrophysics (IP) program, and the lithosaturation panels were displayed. Fig. 5 displays the vertical configuration of the petrophysical parameters and the lithosaturation, which includes the lithological composition, effective porosity, and fluid saturations. The obtained logs were utilized to construct facies and petrophysical models for the Abu Roash members and Bahariya Formation. The shale composition in the layers was determined by utilizing GR, neutron, and density logs. The shale concentration ($V_{sh}$) ranged from 18% to 57% for the Abu Roash C component, 3%–30% for Abu Roash D, 18%–36% for Abu Roash E, 5%–19% for Abu Roash F, 5%–41% for Abu Roash G, and 16%–44% in the Bahariya Formation. The effective porosity was determined by utilizing neutron, density, and sonic logs in conjunction with resistivity logs. This allowed for the identification of fluids and the estimation of their saturations. The Abu Roash "C" has effective porosity values ranging from 20% to 26%, whereas the Abu Roash "D" possesses effective porosity values ranging from 20% to 24%. The porosity values for Abu Roash "E", "F", "G", and Bahariya Formation range from 20%–26%, 19%–22%, 6%–24%, and 15%–26%, respectively. The estimated oil saturation values for the formations analyzed are as follows: 45%–79% for Abu Roash C, 46%–79% for Abu Roash D, 49%–77% for Abu Roash E, 43%–81% for Abu Roash F, 46%–75% for Abu Roash G, and 46%–77% for the Bahariya Formation. Table 1 presents a comprehensive summary of all the petrophysical parameters that have been computed for each level.

### 4.2. Seismic interpretation

Fig. 6 interprets a seismic section that extends from northeast to southwest. It illustrates the faults that impact the area under study. The seismic section demonstrates that normal faults create step faults, which are accompanied by horsts, graben formations, and blocks that are slanted at an angle. The examined section reveals that faults F1, F7, F8, and F9 are normal, with a northeast-facing side (Fig. 6). However, faults F2, F3, F4, F5, and F6 show a typical SW-trending hanging wall. Time-structure maps were created for the horizons of the Abu Roash members and the Bahariya Formation. Next, we conducted a time-depth conversion to generate depth-structure maps for the same horizons. The temporal-depth correlation that is used for time-depth conversion is shown in Fig. 7. According to the structural maps created from seismic data, there were three major tectonic movements in the area, which resulted in the formation of three fault lines (Fig. 8). The initial trend observed is the NW–SE trend, referred to as the Gulf of Suez trend. The second trend is the east-west direction of the Mediterranean, and the third trend is the NNW–SSE alignment, which shows that plate movements occurred from the Paleozoic to the Triassic periods [44]. The depth-structure-contour maps of the Abu Roash members and the Bahariya Formation demonstrate this. After that, the maps were used to create a structural model for the reservoirs in Abu Sennan that were evaluated.

### 4.3. Reservoir modeling

The following step, horizon-making, uses the previously constructed depth maps. The layering process assigns a finer vertical resolution to each zone through the cell thickness. Fig. 9 shows an intersection through the 3D structure model built for the field. As revealed by this intersection, the field is affected by

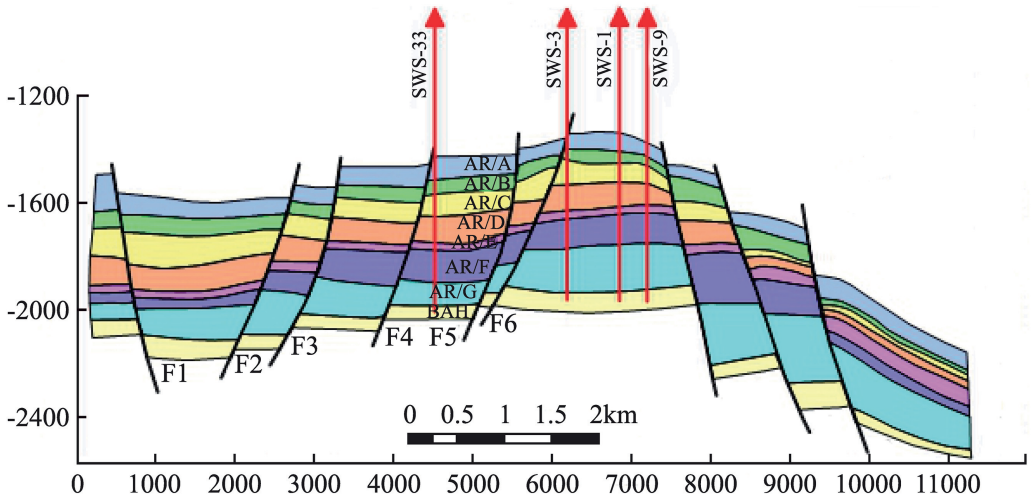


**Fig. 9.** NE–SW-trending intersection through the fields' 3D structural model revealing the faults.

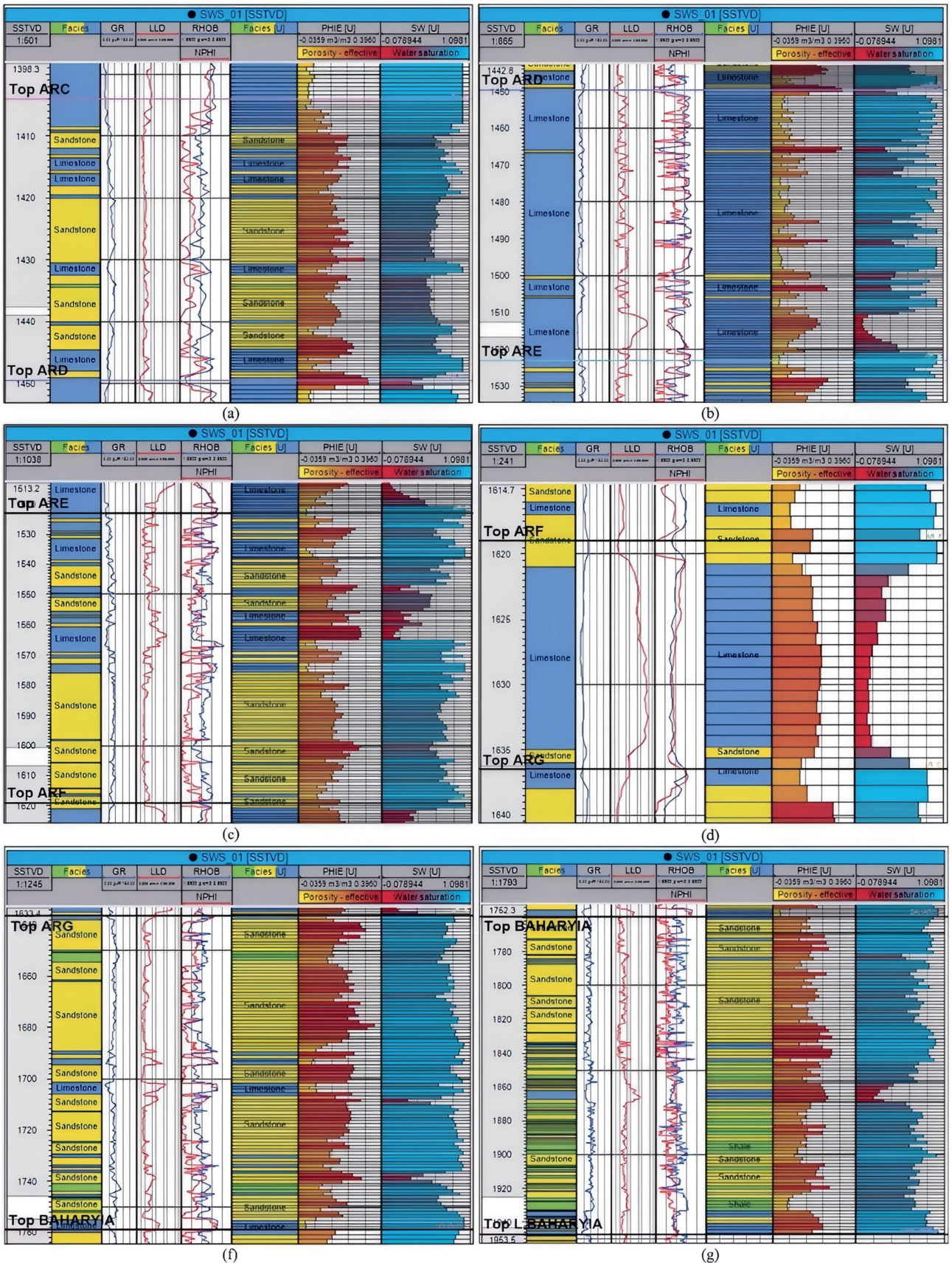


**Fig. 10.** A correlation panel between the discrete facies log on the left and upscaled facies, effective porosity, and hydrocarbon saturation (from left to right): (a) property vertical distribution ARC, (b) property vertical distribution ARD, (c) property vertical distribution ARE, (d) property vertical distribution ARF, (e) property vertical distribution ARG, (f) property vertical distribution Baharyia.

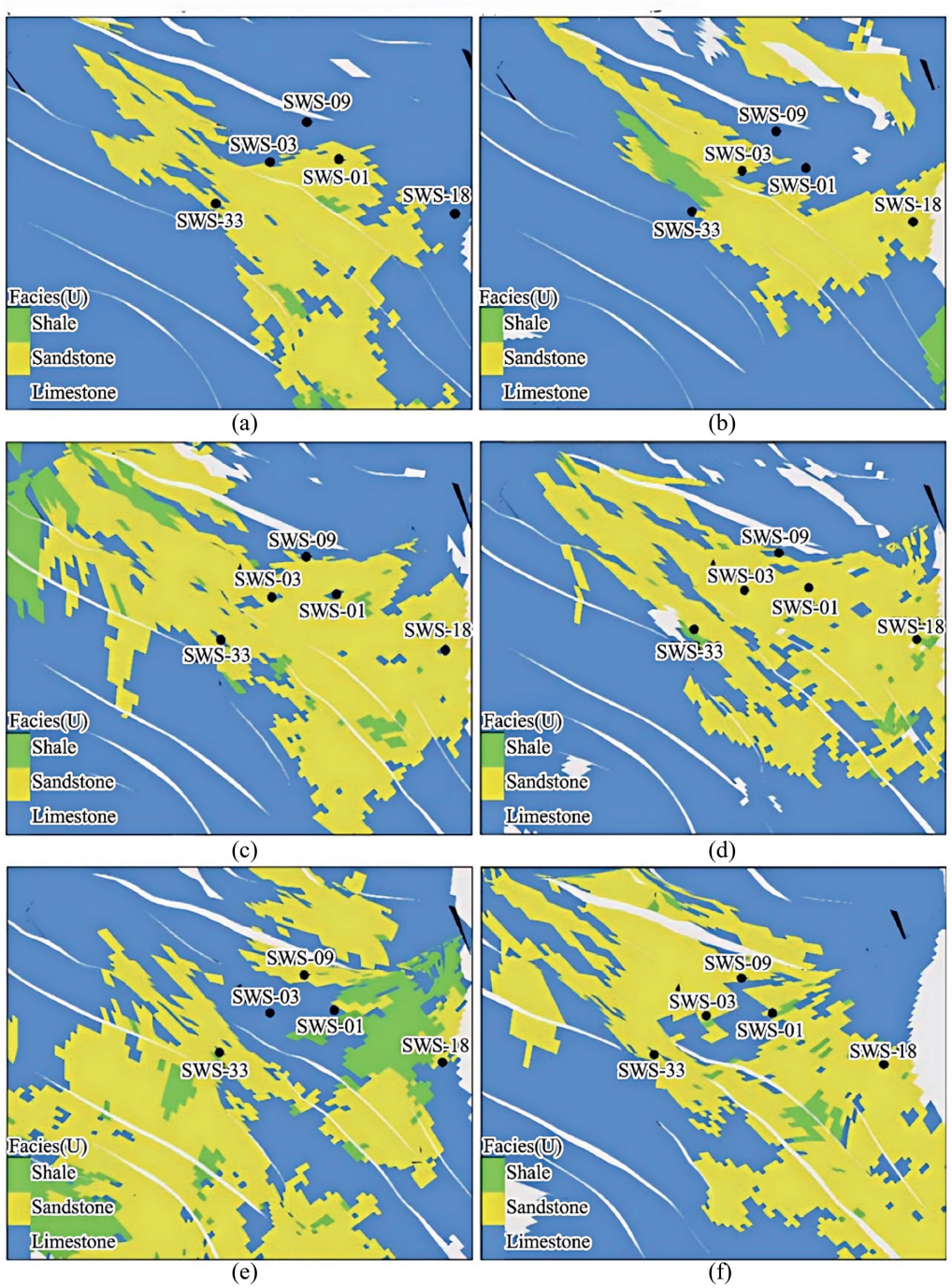


**Fig. 11.** The facies model on top: (a) Abu Roash C, (b) Abu Roash D, (c) Abu Roash E, (d) Abu Roash F, (e) Abu Roash G members, and (f) the Bahariya Formation.

normal faults from NE to SW, step faults, followed by a horst, playing a vital role as a potential structural trap in the field and providing a suitable place, up-dip, for hydrocarbon accumulation. Three facies (sandstone, limestone, and dolomite) were identified in the interval from the Abu Roash "C" (top) to the Bahariya Formation (bottom). A correlation between the discrete facies log, upscaled facies, porosity, and saturation is accomplished (Fig. 10). Fig. 11 shows the facies model at the top of the Abu Roash members and the Bahariya Formation. In Abu Roash C, D, E, and F, sandstone (yellow color) and shale (green color) facies are distributed in the central part, whereas the limestone (blue color) facies occupy the outer parts. Figs. 12 and 13 show the porosity and saturation models of the Abu Roash members ("C", "D", "E", "F", and "G") and the Bahariya Formation, respectively. The calculated volumes are tabulated for all studied reservoirs (Table 2).

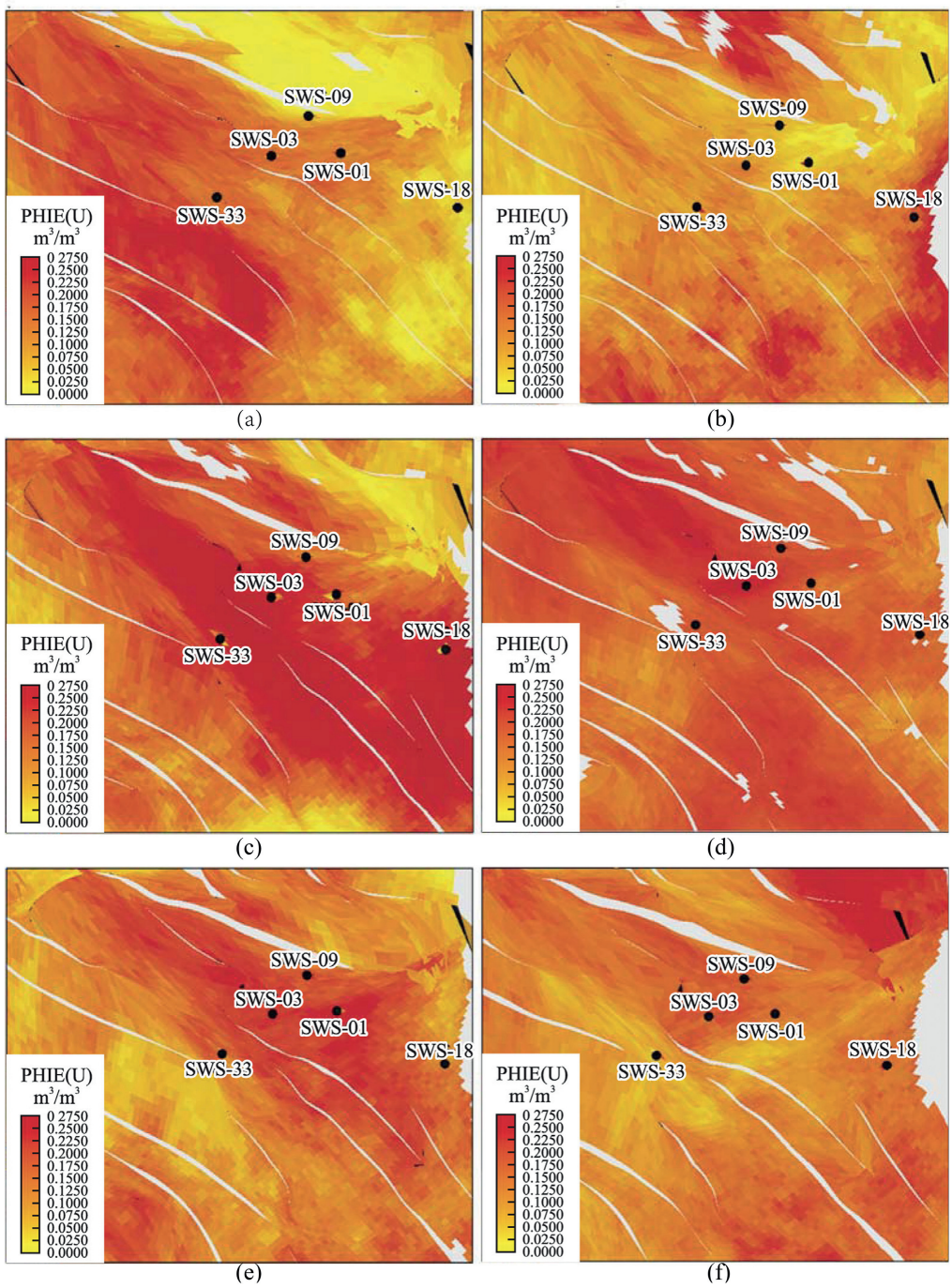


**Fig. 12.** The effective porosity model on top: (a) Abu Roash C, (b) Abu Roash D, (c) Abu Roash E, (d) Abu Roash F, (e) Abu Roash G members, and (f) the Bahariya Formation.

### *4.4. Prospect generation*

A comprehensive integration between the structural analysis, structure, facies, and property models was accomplished to develop the studied field and generate new prospects in the study area. The proposed prospects are outlined on the models' intersections (Fig. 14). The newly suggested prospects were chosen to have the criteria for a suitable reservoir, and they were chosen on the up-thrown sides of the faults and were of good reservoir quality. The new prospects have low shale content, proper effective porosity, and beneficial oil saturation.

## 5. Discussion

The Bahariya Formation comprises sandstone with shale intercalations, consistent with what is stated by Ref. [72]. The Bahariya Formation is a source rock, as reported by Ref. [73], and a promising reservoir rock, as stated by Ref. [73]. The Abu

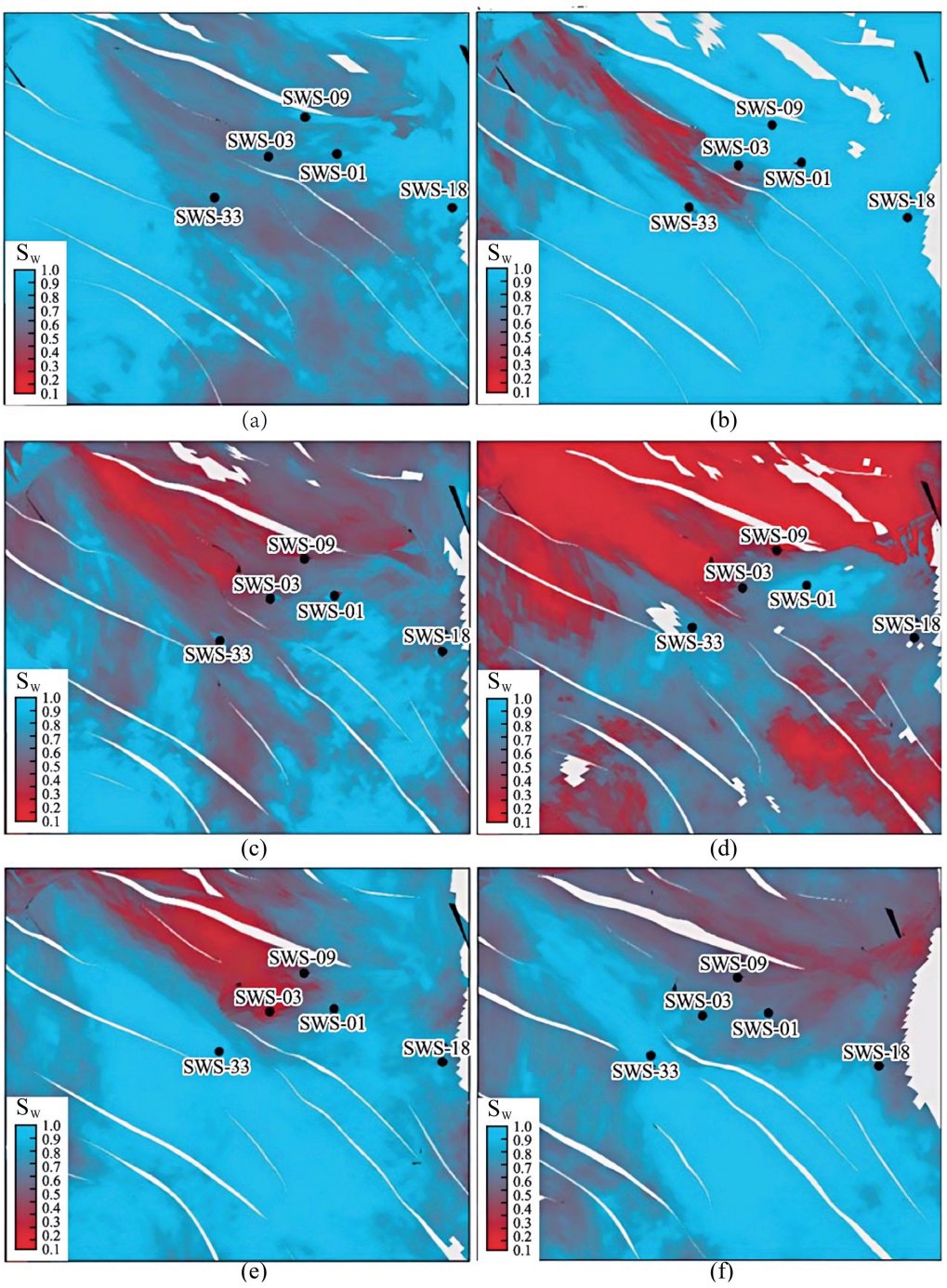


**Fig. 13.** The saturation model on top: (a) Abu Roash C, (b) Abu Roash D, (c) Abu Roash E, (d) Abu Roash F, (e) Abu Roash G members, and (f) the Bahariya Formation.

Roash Formation, overlaying the Bahariya Formation, comprises limestone and sand with shale intercalations. It is subdivided into seven members, from "A" at the top to "G" at the bottom. This comprehensive study recognized and mapped the structure-affected Abu Sennan area. The seismic interpretation revealed various structural regimes from that of other authors [19,31]. This interpretation showed that no reverse faults exist in this portion of the study area. The first trend is the NW–SE trend (Gulf of Suez trend), the second is the east–west trend of the Mediterranean, and the third is the NNW–SSE trend representing the tectonic movement of the Paleozoic to Triassic, according to Ref. [44], as illustrated from the depth-structure-contour maps of the investigated reservoirs. This study further evaluated the area's petrophysical parameters of the Abu Roash

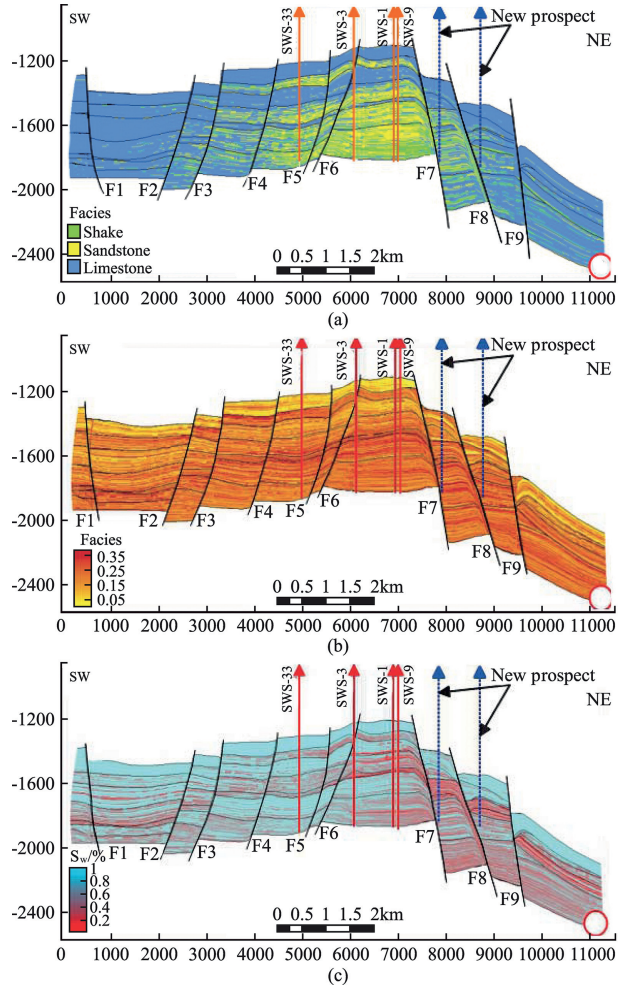


**Fig. 14.** NE–SW-trending cross-sections showing: (a) facies, (b) effective porosity, and (c) hydrocarbon saturation models, highlighting the proposed new prospects with blue dashed lines.

**Table 2**
The estimated stock oil in place (with P50) of the promising reservoirs in the field.

| Formation/menber | Pore volume ($\times 10^6$ rm$^3$) | STOIIP[a] (in oil) ($\times 10^6$ sm$^3$) |
|---|---|---|
| AR/E | 1189 | 394 |
| AR/F | 508 | 216 |
| AR/G | 1825 | 376 |
| Upper Baharyia | 2118 | 601 |

[a] STOIIP: stock tank oil initially in place.

and Bahariya Formations. Unlike, [43], this work studied Abu Roash and Bahariya formations. Besides, it included building 3D static reservoir modeling.

## 6. Conclusions

All available data in Abu Sennan were used to build a 3D static reservoir modeling for potential reservoirs. Geophysical well records aided in determining the lithological compositions and evaluating the primary petrophysical parameters of the Abu Roash and Bahariya Formations. The Abu Roash members primarily comprise carbonate, shale, and sandstone rocks, and the Bahariya Formation comprises sandstone with shale intercalations. The shale concentration ($V_{sh}$) ranged from 18% to 57% in the Abu Roash "C", from 3% to 30% in Abu Roash "D", from 18% to 36% in Abu Roash "E", from 5% to 19% in Abu Roash "F", from 5% to 41% in Abu Roash "G", and from 16% to 44% in the Bahariya Formation. Abu Roash "E" and "G" and the Bahariya Formation are the most promising reservoirs in Abu Sennan. The effective porosity values of the Abu Roash "C" component range from 20% to 26%, whereas the Abu Roash "D" has values ranging from 20% to 24%. The effective porosity values for Abu Roash E, F, G, and Bahariya Formation range from 20% to 26%, 19%–22%, 6%–24%, and 15%–26%, respectively. The estimated oil saturation values for the formations analyzed are as follows: 45%–79% for Abu Roash C, 46%–79% for Abu Roash D, 49%–77% for Abu Roash E, 43%–81% for Abu Roash F, 46%–75% for Abu Roash G, and 46%–77% for the Bahariya Formation. Abu Roash "E" and "G" and the Bahariya Formation are the most promising reservoirs in Abu Sennan. The given 3D seismic data were used to trace the targeted horizons and pick the faults affecting the area. The picked horizons and faults were used to create depth-structure contour maps. The geophysical well logs, the estimated petrophysical parameter logs, and the seismic-derived depth-structure maps are essential components of the built 3D static reservoir modeling. The constructed structural, facies, and petrophysical models were used to calculate the OIIP and delineate new prospects for further drilling and field development. Abu Roash "E" and "G" and the Bahariya Formation have beneficial oil volumes, and two new prospects are recommended for field development.

## CRediT authorship contribution statement

**Taher Mostafa:** Writing – original draft, Resources, Methodology, Formal analysis, Data curation. **Mohamed Reda:** Writing – review & editing, Visualization, Software, Investigation, Data curation. **Mohamed Mosaad:** Writing – original draft, Validation, Software, Formal analysis, Data curation, Conceptualization. **Dmitriy Martyushev:** Writing – original draft, Supervision, Resources, Methodology, Data curation. **Mansour H. Al-Hashim:** Writing – review & editing, Validation, Software, Resources. **Mohamed Fathy:** Writing – review & editing, Visualization, Validation, Formal analysis, Data curation.

## Data availability

The data supporting the conclusions of this study may be obtained from the corresponding author upon a reasonable request.

## Ethical statements

The manuscript has not been submitted or published anywhere, in whole or in part. In other words, the authors confirm that the article is unique. The manuscript will not be submitted to any other publication until the editorial process has been finished.

## Funding

This research was supported by the Researchers Supporting Project number (**RSPD2025R781**), King Saud University, Riyadh, Saudi Arabia; This research was funded by the Ministry of Science and Higher Education of the Russian Federation (Project No. FSNM-2024-0005).

## Declaration of competing interest

The authors declare that they have no known competing financial interests or personal relationships that could have appeared to influence the work reported in this paper.

## Acknowledgments

The authors extend their appreciation to the Researchers Supporting Project number (**RSPD2025R781**), King Saud University, Riyadh, Saudi Arabia. The authors express their gratitude to the Egyptian General Petroleum Corporation and General Petroleum Company for supplying the necessary raw materials and geochemical reports from their archives. They are also grateful for the provision of digital logs and permission to publish.

## References

[1] W.S. El Diasty, S.Y. El Beialy, R. Littke, F.A. Farag, Source rock evaluation and nature of hydrocarbons in the Khalda concession , Shushan basin , Egypt ' s Western Desert, Int. J. Coal Geol. 162 (2016) 45–60, https://doi.org/10.1016/j.coal.2016.05.015.

[2] A. Saad, T.A. Fattah, H. Holial, A.I. Diab, S. Abou Shagar, Exploration of new hydrocarbon leads in the eastern flank of Abu Gharadig Basin, north Western Desert, Egypt, Alex. Eng. J. 66 (2023) 669–690.

[3] M.I. Abdel-Fattah, M. Reda, M. Fathy, D.A. Saadawi, F. Alshehri, M.S. Ahmed, Oil-source correlation and Paleozoic source rock analysis in the Siwa Basin, Western Desert: insights from well-logs, Rock-Eval pyrolysis, and biomarker data, Energy Geosci (2024) 100298, https://doi.org/10.1016/j.engeos.2024.100298.

[4] M. Mamdouh, M. Reda, M.Y.Z. El Din, T.H. Abdelhafeez, 3D petroleum reservoir modelling using seismic and well-log data to assess hydrocarbon potential in Abu Roash (G) Member, Karama Oil Field, North-Western Desert, Egypt, Geol. J. 59 (1) (2024) 313–324.

[5] M.I. Abdel-Fattah, M.A. Sarhan, A.S. Ali, H.A. Hamdan, Structural and petrophysical characteristics of the Turonian "AR/G ″reservoirs in heba field (Western Desert, Egypt): integrated approach for hydrocarbon exploration and development, J. Afr. Earth Sci. 207 (2023) 105072.

[6] D.W. Lewis, D. McConchie, Practical Sedimentology, second ed., Springer Science+Business Media Dordrecht, 1994 https://doi.org/10.1007/978-1-4615-2634-6.

[7] M.D. Blum, S.B. Marriott, S.F. Leclair, I. Jarvis, *Fluvial Sedimentology VII*. International Association of Sedimentologists and Published for Them, Blackwell Publishing Ltd, 2005, https://doi.org/10.1002/9781444304213.

[8] D.A. Martyushev, S. Davoodi, A. Kadkhodaie, M. Riazi, Y. Kazemzadeh, T. Ma, Multiscale and diverse spatial heterogeneity analysis of void structures in reef carbonate reservoirs, Geoenergy Science and Engineering 233 (2024) 212569, https://doi.org/10.1016/j.geoen.2023.212569.

[9] E.A. Gawad, M. Fathy, M. Reda, H. Ewida, Re-evaluation of the oil potentiality of Matulla Formation in October oil field, Gulf of Suez, Egypt, using the 3D static reservoir modeling of well logs and seismic data, Egypt. J. Appl. Geophys. Egypt, Egypt. Soc. Appl. Petrophysics 18 (2) (2019) 21–34.

[10] E.A. Gawad, M. Fathy, M. Reda, H. Ewida, 3D static reservoir modeling, using well logs and seismic data, to reevaluate the oil potentiality of the Upper Rudeis Formation (Asl member) in October oil field, Gulf of Suez, Egypt, Ann. Geol. Surv. Egypt, Egypt. Miner. Resour. Authority XXXIIV (2020) 216–237.

[11] M. Reda, M. Fathy, E.A. Gawad, Comprehensive 3D reservoir modelling and basin analysis: an insight into petroleum geology, to reevaluate the hydrocarbon possibilities in the Siwa Basin, North Western Desert, Egypt, Geol. J. 57 (4) (2022) 1600–1616, https://doi.org/10.1002/gj.4362.

[12] M.M. El Nady, Timing of petroleum generation and source maturity of selected wells in Abu Gharadig Basin, north Western Desert, Egypt, Energy Sources 38 (3) (2016) 391–401, https://doi.org/10.1080/15567036.2013.784832.

[13] A. El-Bassiony, M. Fahmy, A. Lotfy, B. Esinov, Imaging the Lower Cretaceous complex fault systems using common reflection angle migration, Abu Gharadiq Basin, Western Desert, Egypt, First Break 41 (5) (2023) 51–55.

[14] S. Hassan, S. Tahoun, M. Darwish, W. Bosworth, A.E. Radwan, The Albian–Cenomanian boundary on the southern Tethyan margin: Abu Gharadig Basin, northern Western Desert, Egypt, Mar. Petrol. Geol. 154 (2023) 106334.

[15] A.M. Noureldin, W.M. Mabrouk, B. Chikiban, A. Metwally, Formation evaluation utilizing a new petrophysical automation tool and subsurface mapping of the Upper Cretaceous carbonate reservoirs, the southern periphery of the Abu-Gharadig basin, Western Desert, Egypt, J. Afr. Earth Sci. (2023) 104977.

[16] E.S. Selim, M.A. Sarhan, New stratigraphic hydrocarbon prospects for the subsurface Cretaceous: tertiary succession within Abu Gharadig Basin in the framework of sequence stratigraphic analyses, north Western Desert, Egypt, Euro-Mediterranean J. Environ. Integr. 8 (4) (2023) 969–986.

[17] W.A. Ali, A.S. Deaf, T. Mostafa, 3D geological and petrophysical modeling of Alam El-Bueib formation using well logs and seismic data in Matruh field, northwestern Egypt, Sci. Rep. 14 (1) (2024) 6849, https://doi.org/10.1038/s41598-024-56825-5.

[18] A. Abo Bakr, H.H. El Kadi, T. Mostafa, Petrographical and petrophysical rock typing for flow unit identification and permeability prediction in lower cretaceous reservoir AEB_IIIG, Western Desert, Egypt, Sci. Rep. 14 (1) (2024) 5656, https://doi.org/10.1038/s41598-024-56178-z.

[19] M.F. Abu-Hashish, H. Hamdalla, E. Madian, 3D geological modeling of the Upper Cretaceous reservoirs in GPT oil field , Abu Sennan area , Western Desert , Egypt, J. Pet. Explor. Prod. Technol. 10 (2) (2020) 371–393, https://doi.org/10.1007/s13202-019-00780-9.

[20] A.M. Noureldin, W.M. Mabrouk, A. Metwally, Delineating tidal channel feature using integrated post-stack seismic inversion and spectral decomposition applications of the upper cretaceous reservoir Abu Roash/C: a case study from Abu-Sennan oil field, Western Desert, Egypt, J. Afr. Earth Sci. (2023) 104974.

[21] A.H. Saleh, A. Henaish, F.S. Ramadan, M.O.A. El Fatah, M. Leila, Petrophysical characterization of the heterogeneous shale-rich oil reservoirs: a case study of the Cenomanian Clastics, Abu sennan concession, north Western Desert of Egypt, Arabian J. Geosci. 16 (6) (2023) 351.

[22] G. Farrag, A. Bakr, A. Abd-Allah, S. El-Shahawy, Seismic criteria and structural styles for half graben differential inversion: implication for hydrocarbon accumulation, Abu Sennan blocks, Western Desert, Egypt, Environ. Geosci. 28 (1) (2021) 33–42.

[23] H.H. Abuseda, A.M.A.A. El Sayed, O.M. Elnaggar, Permeability modeling of upper cretaceous Bahariya Formation rocks, Abu Sennan field, Western Desert, Egypt, Arabian J. Geosci. 16 (3) (2023) 211.

[24] A. Helba, W. Ali, M.A. Fattah, H. Mokhtar, M. Farouk, Poroperm characterization and rock typing of tight carbonate reservoir using core calibrated image perm technique: turonian carbonates in Abu sennan field, Western Desert, Egypt, A case study, in: *SPE North Africa Technical Conference and Exhibition*, SPE, 2015 D031S024R002.

[25] A. Sultan, et al., Integration between well logging and seismic reflection techniques for reservoir evaluation of Abu roash "C", Abu sennan area, Abugharadig basin, Western Desert of Egypt, in: *Offshore Mediterranean Conference and Exhibition*, OMC, OMC-2021, 2021.

[26] A.A. Shehata, M.A. Sarhan, Seismic interpretation and hydrocarbon assessment of the post-rift Cenomanian Bahariya reservoir, beni suef basin, Egypt, J. Pet. Explor. Prod. Technol. 12 (12) (2022) 3243–3261.

[27] A.A. Shehata, M.A. Sarhan, M.I. Abdel-Fattah, S. Mansour, Geophysical assessment for the oil potentiality of the Abu roash 'G' reservoir in west beni suef basin, western Desert, Egypt, J. Afr. Earth Sci. 199 (2023) 104845.

[28] M.A. Taha, T.H. Abdelhafeez, S.M. El-hady, A.Z. Nooh, W.H. Mohamed, Improving hydrocarbon prospect evaluation at Badr El Din-3 and Badr El Din-15 oil fields by integrating 3D structural modeling and petrophysical analysis for Abu-Gharadig basin , north of Western Desert , Egypt, Arabian J. Sci. Eng. (2022), https://doi.org/10.1007/s13369-022-07038-3.

[29] M.A. Abd El-Hady, T.A. Hamed, M.A. Abdelwahhab, A new hydrocarbon prospect determination through subsurface and petrophysical evaluation of Abu Roash 'G' member in Abu Sennan area, North Western Desert, Egypt, Nat. Sci. 12 (11–30) (2014) 199–218.

[30] M.A. Abd El-Hady, T.A. Hamed, M.A. Abdelwahhab, A new prospective hydrocarbon determination via subsurface and petrophysical evaluation of the turonian Abu Roash 'E' member in Abu sennan area, north Western Desert, Egypt, J. Geol. 59 (2015).

[31] W.S. El Diasty, J.M. Moldowan, Application of biological markers in the recognition of the geochemical characteristics of some crude oils from Abu Gharadig Basin, north Western Desert – Egypt, Mar. Petrol. Geol. 35 (1) (2012) 28–40, https://doi.org/10.1016/j.marpetgeo.2012.03.001.

[32] M.A. Abdelwahhab, E.H. Ali, N.A. Abdelhafez, Petroleum system analysis-conjoined 3D-static reservoir modeling in a 3-way and 4-way dip closure setting: insights into petroleum geology of fluvio-marine deposits at BED-2 Field (Western Desert, Egypt), Petroleum 9 (1) (2023) 8–32, https://doi.org/10.1016/j.petlm.2021.06.001.

[33] R. Turner, M. Ahmed, R. Bissell, L.O. Prothro, A.A. Shehata, R. Coffin, Structural and stratigraphic controls on reservoir architecture: a case study from the lower Oligocene Vicksburg Formation, Brooks County, Texas, Mar. Petrol. Geol. 160 (2024) 106627.

[34] M. Abukliesh, T. Mostafa, M.Y.Z. El Din, T.H. Abdelhafeez, 3D seismic data interpretation and static reservoir modeling of Mamuniyat formation, I and R oil fields, Murzuq basin, Libya, Iraqi Geol. J. (2024) 275–286.

[35] M. Abukliesh, T. Mostafa, Z. El Din, T.H. Abdelhafeez, Integrating well logs and core data for Better reservoir characterization of Mamuniyat formation, Murzuq basin, Libya, Iraqi Geol. J. (2024) 1–10.

[36] A.A. Shehata, M.I. Abdel-Fattah, H.A. Hamdan, M.A. Sarhan, Seismic interpretation and sequence stratigraphic analysis of the Bahariya Formation in the South Umbaraka oilfields (Western Desert, Egypt): insights into reservoir distribution, architecture, and evaluation, Geomech. Geophys. Geo-Energy Geo-Resources 9 (1) (2023) 135.

[37] S.M.T. Qadri, M.A. Islam, M.R. Shalaby, Three-dimensional petrophysical modelling and volumetric analysis to model the reservoir potential of the Kupe Field, Taranaki Basin, New Zealand, Nat. Resour. Res. 28 (2019) 369–392.

[38] A.O. Adelu, et al., Application of 3D static modeling for optimal reservoir characterization, J. Afr. Earth Sci. 152 (2019) 184–196.

[39] S.M.T. Qadri, M.A. Islam, M.R. Shalaby, S.H. Ali, Integration of 1D and 3D modeling schemes to establish the farewell Formation as a self-sourced reservoir in Kupe field, Taranaki basin, New Zealand, Front. Earth Sci. (2020) 1–18.

[40] S.M.T. Qadri, W. Ahmed, A.K.M.E. Haque, A.E. Radwan, M.H. Hakimi, A.K. Abdel Aal, Murree clay problems and water-based drilling mud optimization: a case study from the Kohat Basin in Northwestern Pakistan, Energies 15 (9) (2022) 3424.

[41] N.A. El Sayeda, A.M.A. El Sayed, Petrophysical modelling for the Bahariya Formation, Egypt, Procedia Earth Planet. Sci. 15 (2015) 518–525, https://doi.org/10.1016/j.proeps.2015.08.068.
[42] C. Octavian, M. Khalifa, H. Wanas, Sequence stratigraphy of the lower Cenomanian Bahariya Formation, Bahariya Oasis, Western Desert, Egypt, Sediment. Geol. 190 (2006) 121–137, https://doi.org/10.1016/j.sedgeo.2006.05.010.
[43] I. Salem, H. Ghazala, W. El, Prospect evaluation of BED 3 and Sitra oilfields , Abu Gharadig Basin , north Western Desert , Egypt, NRIAG J. Astron. Geophys. 4 (2) (2015) 222–235, https://doi.org/10.1016/j.nrjag.2015.09.002.
[44] W. Meshref, H. Hammauda, Magnetic and gravity investigation of deep oil prospects in the Gulf of Suez, in: SEG Technical Program Expanded Abstracts 1982, 2005, pp. 365–367, https://doi.org/10.1190/1.1826979.
[45] A.M. El Gazzar, A.R. Moustafa, P. Bentham, Structural evolution of the Abu Gharadig field area, northern Western Desert, Egypt, J. Afr. Earth Sci. 124 (2016) 340–354, https://doi.org/10.1016/j.jafrearsci.2016.09.027.
[46] W. Bosworth, G. Tari, Hydrocarbon accumulation in basins with multiple phases of extension and inversion: examples from the Western Desert (Egypt) and the Western Black Sea, Solid Earth (12) (2021) 1–19, https://doi.org/10.5194/se-12-59-2021.
[47] T.F. Shazly, A.Z. Nouh, Determination of some reservoir characteristics of the Bahariya Formation in Bed-1 field , Western Desert , Egypt , by using the repeat formation tester, Petrol. Sci. Technol. 31 (7) (2013) 763–774, https://doi.org/10.1080/10916466.2010.531603.
[48] M. Halisch, A. Weller, C. Sattler, W. Debschütz, A.M. El-sayed, A complex core-log case study of an anisotropic sandstone , originating from Bahariya Formation , Abu Gharadig Basin , Egypt, Petrophysics 50 (December) (2015) 478–497.
[49] I. Salem, H. Ghazala, W. El Diasty, Prospect evaluation of BED 3 and Sitra oilfields, Abu Gharadig Basin, north Western Desert, Egypt, NRIAG J. Astron. Geophys. 4 (2) (2015) 222–235, https://doi.org/10.1016/j.nrjag.2015.09.002.
[50] T.R. El-Qalamoshy, M.I. Abdel-Fattah, M. Reda, T.H. Abdelhafeez, S.S.S. Azzam, M. Mosaad, A multi-disciplinary approach for trap identification in the Southern Meleiha Area, North Western Desert, Egypt: integrating seismic, well log, and fault seal analysis, Geomech. Geophys. Geo-Energy Geo-Resources 9 (1) (2023) 157.
[51] M. Reda, T. Mostafa, A. Raef, M. Fathy, F. Alshehri, M. Ahmed, Hydrocarbon Reservoir Characterization in the Challenging Structural Setting of Southern Gulf of Suez: Synergistic Approach of Well Log Analyses and 2D Seismic Data Interpretation, 2024.
[52] M. Reda, M. Fathy, E.A. Gawad, Comprehensive 3D reservoir modelling and basin analysis: an insight into petroleum geology to re-evaluate the hydrocarbon possibilities in the Siwa Basin, North-Western Desert, Egypt, Geol. J. 57 (4) (2022) 1600–1616.
[53] A. Bakr, M. Reda, M. Fathy, Application of 3D static modelling and reservoir characterisation for optimal field development: a case study from the Kharita Formation, Karam field, Western Desert, Egypt, First Break 41 (11) (2023) 43–51.
[54] M.A. Younes, Crude Oil Exploration in the World, IntechOpen, London, United Kingdom, 2012, https://doi.org/10.5772/2676.
[55] E. G. P. C. (EGPC), Western Desert, oil and gas fields (A comprehensive overview), in: EGPC 11th Petroleum Exploration and Production Conference, 1992, p. 431.
[56] S.M.T. Qadri, M.A. Islam, M.R. Shalaby, Application of well log analysis to estimate the petrophysical parameters and evaluate the reservoir quality of the Lower Goru Formation, Lower Indus Basin, Pakistan, Geomech. Geophys. Geo-Energy Geo-Resources 5 (2019) 271–288.
[57] S.M.T. Qadri, M.A. Islam, M.R. Shalaby, A.K.A. El-Aal, Reservoir quality evaluation of the Farewell sandstone by integrating sedimentological and well log analysis in the Kupe South Field, Taranaki Basin-New Zealand, J. Pet. Explor. Prod. 11 (2021) 11–31.
[58] M.A. Abd Elhady, M. Fathy, T. Hamed, M. Reda, Petroleum evaluation through subsurface and petrophysical studies of Hammam Faraun member of Belayim formation, Bakr oil field, Gulf of Suez, Egypt, Nat. Sci. 13 (4) (2015) 59–78.
[59] M. Reda, M. Fathy, M. Mosaad, F. Alshehri, M.S. Ahmed, 3D static modeling and sequence stratigraphy using well logs and seismic data: an example of Abu Roash G member in Bahga oilfield, Energy Geosci 5 (3) (2024) 100303.
[60] T.R. El-Qalamoshy, T.H. Abdelhafeez, S. Shebl, M. Reda, M. Mossad, Detecting Fault trends using seismic attributes: a case study of the southern part of Meleiha, north Western Desert, Egypt, Al-Azhar Bull. Sci. 34 (3) (2024) 9.
[61] Schlumberger, *Log Interpretation Charts*, 2009th ed., Schlumberger, 2009.
[62] Schlumberger, Well Evaluation Conference. Egypt, Schlumberger & EGPC, 1995.
[63] Schlumberger, Introduction to Well Testing, Schlumberger, 1998, https://doi.org/10.1142/9781848160736_0001.
[64] G.R. Pickett, Pattern recognition as a means of formation evaluation, Log. Anal. 14 (4) (1973).
[65] H.W.R. Clavier, D. Meunier, Quantitative interpretation of TDT logs; Part 1 and 11, J. Petrol. Technol. (6) (1971).
[66] E. Makarian, A.B.M.N. Abad, et al., An efficient and comprehensive poroelastic analysis of hydrocarbon systems using multiple data sets through laboratory tests and geophysical logs: a case study in an iranian hydrocarbon reservoir, Carbonates Evaporites 38 (2023) 37, https://doi.org/10.1007/s13146-023-00861-1.
[67] E.A. Gawad, M. Fathy, M. Reda, H. Ewida, Source rock evaluation of the Central Gulf of Suez, Egypt: a 1D basin modelling and petroleum system analysis, Geol. J. 56 (7) (2021) 3850–3867.
[68] E.A. Gawad, M. Fathy, M. Reda, H. Ewida, Petroleum geology: 3D reservoir modelling in the central Gulf of Suez, Egypt, to estimate the hydrocarbon possibility via petrophysical analysis and seismic data interpretation, Geol. J. 56 (10) (2021) 5329–5342.
[69] A. Mansour, T. Gentzis, M. El Nady, F. Mostafa, S. Tahoun, Hydrocarbon potential of the Albian-early Cenomanian formations (Kharita-Bahariya) in the north Western Desert, Egypt: a review, J. Pet. Sci. Eng. 193 (2020) 107440, https://doi.org/10.1016/j.petrol.2020.107440.
[70] D.A. Martyushev, I.N. Ponomareva, et al., Deformation of the void space of pores and fractures of carbonates: comprehensive analysis of core and field data, Energy Geoscience 6 (1) (2025) 100364, https://doi.org/10.1016/j.engeos.2024.100364.
[71] R. Brackenridge, V. Demyanov, O. Vashutin, R. Nigmatullin, Improving subsurface characterisation with 'Big data' mining and machine learning, Energies 15 (Jan. 2022) 1070, https://doi.org/10.3390/en15031070.
[72] R. Said, The Geology of Egypt, A.A.Balkema, Rotterdam, 1990.
[73] M. El Nady, M. Hammad, Evaluation of cretaceous hydrocarbon source rock in Badr El Din concession, north Western Desert, Fuel 20 (2000) 25–51.